Pergamon

Geochimica et Cosmochimica Acta, Vol. 68, No. 13, pp. 2781–2790, 2004

0016-7037/04 $30.00 + .00

doi:10.1016/j.gca.2003.12.007

Constraining the equation of state of fluid H_2O to 80 GPa using the melting curve, bulk modulus, and thermal expansivity of Ice VII

MARK R. FRANK,[1,2,*] YINGWEI FEI,[1] and JINGZHU HU[1]

[1]Geophysical Laboratory, Carnegie Institution of Washington, 5251 Broad Branch Road, Washington, DC 20015, USA
[2]X17C Building 725, Brookhaven National Laboratory, Upton, NY 11973, USA

(*Received February* 25, 2003; *accepted in revised form December* 3, 2003)

Abstract—The study presented here sought to determine the *PVT* properties of Ice VII at elevated temperatures and pressures up to 60 GPa using a Mao-Bell type diamond anvil cell with an external Mo-wire resistance heater. The unit cells of Ice VII and gold were monitored during the experiment with gold being used as an internal pressure calibrant. Additionally, the melting curve of Ice VII was determined to greater than 40 GPa by using the disappearance of the diffraction pattern of Ice VII to monitor melting in the system. The melting curve for Ice VII from 3 to 60 GPa was found to be accurately related by a Simon equation:

$$\frac{(P - 2.17)}{0.764} = \left(\frac{T}{355}\right)^{4.32} - 1$$

where pressure and temperature are denoted by P (GPa) and T (kelvin), respectively.

These results were used further to constrain the *PVT* properties of fluid H_2O at elevated pressures and temperatures by taking the pressure derivative of the Gibbs free energy difference between Ice VII and fluid H_2O along the Ice VII melting curve. Comparison of these results suggests that the previously stated equations of state of fluid H_2O overestimate the molar volume of fluid H_2O at pressures greater than 20 GPa. Although the data presented in this study is not enough to provide an independent *EOS* for fluid H_2O, future work should take account of our data.

1. INTRODUCTION

The physical properties of both solid and fluid H_2O are important geologically over a large range of pressure and temperature. Jupiter's icy satellites are but one illustration of the abundance and importance of solid H_2O phases in planetary physics. Many studies (Consolmagno and Lewis, 1976; Reynolds and Cassen, 1979; Schubert et al., 1981; Anderson et al., 1998; Kuskov and Kronrod, 2001; Scott et al., 2002) have postulated on the internal structure of these satellites with most concluding that high-pressure polymorphs of H_2O are a major component. The significance of high-pressure H_2O polymorphs may not be limited to icy bodies; Bina and Navortsky (2000) have hypothesized that Ice VII could be important in cold subducting slabs in planetary bodies such as Mars. Therefore, high-pressure data in the H_2O system are critical for understanding many planetary processes.

A recent study by Datchi et al. (2000) obtained data on the melting curve of Ice VII up to 13.09 GPa. Their melting curve, extrapolated to higher pressures, predicts much higher melting temperatures than those of Fei et al. (1993), Mishima and Endo (1978) and Pistorius et al. (1963), all of which are congruous. For example, Datchi et al. (2000) predict a melting temperature of approximately 1100 K at 40 GPa whereas Fei et al. (1993) predicts approximately 800 K. The large discrepancy present in the extrapolation of these studies to high pressure results in an unacceptable level of uncertainty that must be addressed before quantitative modeling is attempted.

Additionally, the physical properties of fluid H_2O are important geologically over a large range of pressure and temperature. Shock-wave data have served as the main resource for the derivations of many equations of state (*EOS*) for fluid H_2O (e.g., Rice and Walsh, 1957; Halbach and Chatterjee, 1982; Saxena and Fei, 1987; Stixrude and Bukowinski, 1990; Belonoshko and Saxena, 1991; Pitzer and Sterner, 1994; Sakane et al., 2001). Direct measurements of the molar volume of water are required to test the validity of these models, however, these measurements at elevated pressures and temperatures are difficult and, as a result, rare. Fei et al. (1993) and Fei and Mao (1993) used the melting curve of Ice VII to constrain the molar volume of fluid H_2O along the melting curve (up to 16 GPa), and found it was broadly consistent with the models mentioned previously to approximately 45 GPa. However, they also noted that the models of Belonoshko and Saxena (1991) and Stixrude and Bukowinski (1990) overestimated the molar volume by approximately 0.5 cm^3/mol at 80 GPa and 950 K. Although Datchi et al. (2000) did not measure the volumetric properties of Ice VII, the disparity in the specific volume of fluid H_2O calculated from their melting curve and the others is significant and needs to be addressed.

The study presented here sought to determine the *PVT* properties of Ice VII at pressures $>$ 20 GPa and especially along the melting curve at high-pressures to further constrain the equation of state of fluid H_2O and to test the models of previous workers derived from low-pressure data and extrapolated to high-pressures.

* Author to whom correspondence should be addressed, at Department of Geology and Environmental Geosciences, Northern Illinois University, Davis Hall 312, Normal Road, DeKalb, IL 60115, USA (mfrank@niu.edu).

2. EXPERIMENTAL AND ANALYTICAL TECHNIQUES

The sample was contained in a Mao-Bell type diamond anvil cell with an external heater. This diamond cell configuration has been described in detail previously (Mao et al., 1991; Fei, 1996), so we limit the discussion here accordingly. The body of the cell is made from Inconel 625, whereas the diamonds (300-350 μm culet, approximately 2.3 mm height) were mounted to tungsten carbide seats on the piston and cylinder. The cell was heated initially to 400-500 K using an external $Ni_{0.8}Cr_{0.2}$-wire resistance heater (34 mm inner diameter, 60 mm outer diameter, 40 mm length) wrapped around the cylinder of the cell. Higher temperatures were obtained using a small Mo-wire resistance heater placed around the diamond anvils in addition to the $Ni_{0.8}Cr_{0.2}$ heater. The small heater was constructed with Mo wire (0.25 mm diameter) wound tightly around an alumina tube (5.5 mm outer diameter, 4.0 mm inner diameter, 2.5 mm thick). The temperature of the experiment was determined by placing a type-S thermocouple ($Pt\text{-}Pt_{0.9}Rh_{0.1}$) between the diamond anvil and Re-gasket, directly against the surface of the diamond. Temperatures were kept constant to ± 5 K during data collection, whereas the uncertainty associated with the thermocouple itself is ± 2 K over the range of temperatures in this study.

Based on the projected temperature and pressure range of this study, rhenium gaskets were utilized. The rhenium gaskets were 3.8 mm in diameter and 0.38 mm thick. The gaskets were preindented to approximately 30 GPa decreasing the thickness of the gasket to approximately 27 μm. Some 70-150 μm holes were drilled in the compressed regions by using an erosion drill. This hole acts as the sample chamber bound on the sides by the Re-gasket and placed between the two diamond anvils. Gold and H_2O were loaded into the sample chamber and compressed, at room temperature, to >5 GPa to seal the contents in the sample chamber.

The experiments were conducted at the Brookhaven National Synchrotron Light Source, beam line X17C superconducting wiggler line using the energy dispersive X-ray diffraction (EDXD) technique. Polychromatic radiation was implemented in the experiments as was two reciprocal perpendicular slits to limit the incident X-ray beam size to approximately 11 by 8 μm. The X-ray energy was calibrated to channels in a solid-state germanium detector by using the X-ray emission energies of Cu, Rb, Mo, Ag, Ba, Tb and Am. The energies are related to *d*-spacings based on the Bragg relation:

$$\text{Energy (keV)} = \frac{6.1993}{d(\text{Å}) \cdot \sin\theta}. \quad (1)$$

The data were collected with the detector at a fixed two-theta angle ($2\theta = 15.003 \pm 0.005°$) that was calibrated by using the diffraction lines of a gold standard. Exposure times were for 1-5 min depending on sample size with smaller and thinner samples requiring longer exposure times.

The diffraction pattern of H_2O and gold were monitored during the experiment. The unit cell of gold determined from the diffraction lines was used in conjunction with a previously established *PVT* equation of state (Anderson et al., 1989) so that gold acted as an internal pressure calibrant. The {111}, {200} and {220} diffraction lines of gold were present in most analyses. The uncertainty in gold unit cell volume calculated from the three diffraction lines was monitored and determined to cause uncertainties in the calculated pressure of 0.1 to 0.4 GPa at pressures below 20 GPa and increased to approximately 1 GPa at pressures of approximately 60 GPa. The variation is thought to be due to the deviatoric stress attributed to the nonhydrostatic environment of the diamond anvil cell (Meng et al., 1993). The uncertainty in unit cell volume, and thus the calculated pressure, was addressed by taking the 2σ standard deviation from the mean of the lattice parameters for gold determined from each of the three lines as the minimum uncertainty. Typically, the uncertainty was approximately 0.2 to 0.8 GPa over the entire pressure range examined. The gold lattice uncertainty was also used to estimate the uncertainty in the measurement of the volume of Ice VII.

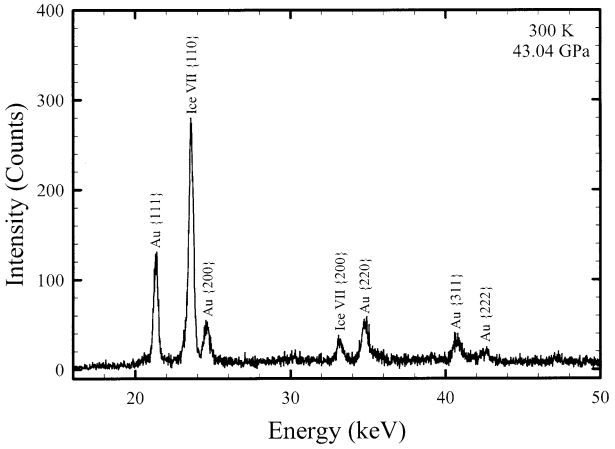

Fig. 1. Energy dispersive X-ray diffraction pattern from experiment 20 of Ice VII and gold (internal pressure calibrant) at 300 K and 43.03 $\pm$ 0.05 GPa. The data were collected as a function of energy (keV) at a $2\theta = 15°$ for approximately 2 min. The diffraction lines associated with gold and Ice VII are labeled and were present in most experiments.

3. EXPERIMENTAL RESULTS

3.1. Isothermal Compression of Ice VII at 300

Figure 1 shows a typical energy-dispersive diffraction pattern of Ice VII and gold. The {110} diffraction line of Ice VII was the strongest diffraction line under almost all conditions and was the primary line used in calculation of the unit cell volume, however, the {200} diffraction line was also used whenever possible. There was good agreement in the Ice VII unit cell volumes calculated from each of the diffraction lines. The 300 K compression data were collected for Ice VII from 6.57 to 60.52 GPa (Fig. 2 and Table 1) and were fit to a third-order Birch-Murnaghan equation of state (Birch, 1978):

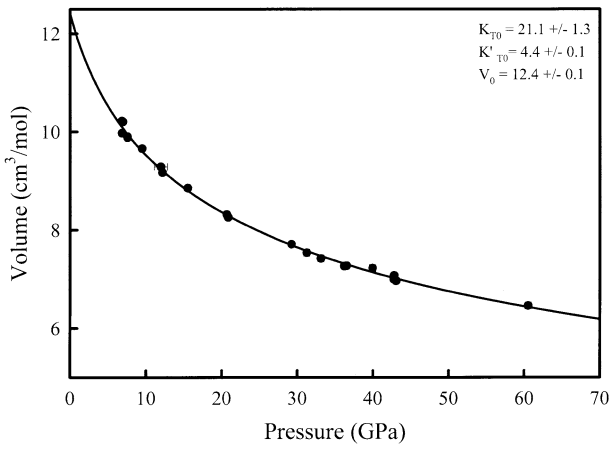

Fig. 2. X-ray data were used to calculated pressure-volume data at 300 K to establish an isothermal compression for Ice VII. The solid circles represent individual data points whereas the error bars are calculated following the methods outlined in the text and are 2σ standard deviation from the mean. A third-order Birch-Murnaghan equation of state was fitted to the data and indicates the zero-pressure volume (V_0), bulk modulus (K_{T0}) and its pressure derivative (K'_{T0}) are12.4 $\pm$ 0.1 (cm^3/mol), 21.1 $\pm$ 1.3 GPa and 4.4 $\pm$ 0.1, respectively.

Table 1. Pressure-volume-temperature data for H_2O–Ice VII collected from 300 to 900 K and 6.8 to 65 GPa.[a]

Experiment	T (K)	P (GPa)	a (Au, Å)	a (Ice VII, Å)	V (Ice VII, cm^3/mol)
1	300	6.82 ± 0.2	4.0286 ± 0.0015	3.2381 ± 0.0012	10.220 ± 0.011
2	300	6.85 ± 0.23	4.0284 ± 0.0015	3.2119 ± 0.0012	9.973 ± 0.011
3	300	6.97 ± 0.2	4.0276 ± 0.0015	3.2367 ± 0.0012	10.206 ± 0.011
4	300	7.56 ± 0.19	4.0238 ± 0.0012	3.2043 ± 0.0010	9.903 ± 0.009
5	300	7.56 ± 0.19	4.0238 ± 0.0012	3.2021 ± 0.0010	9.883 ± 0.009
6	300	9.49 ± 0.11	4.0116 ± 0.0007	3.1778 ± 0.0006	9.659 ± 0.005
7	300	11.95 ± 0.87	3.9969 ± 0.0050	3.1366 ± 0.0039	9.289 ± 0.035
8	300	12.16 ± 0.20	3.9957 ± 0.0012	3.1235 ± 0.0009	9.172 ± 0.008
9	300	15.48 ± 0.3	3.9772 ± 0.0015	3.0872 ± 0.0012	8.856 ± 0.010
10	300	20.65 ± 0.38	3.9509 ± 0.0018	3.0230 ± 0.0014	8.315 ± 0.011
11	300	20.86 ± 0.11	3.9499 ± 0.0005	3.0159 ± 0.0004	8.257 ± 0.003
12	300	29.23 ± 0.20	3.9126 ± 0.0008	2.9482 ± 0.0006	7.713 ± 0.005
13	300	31.24 ± 0.4	3.9044 ± 0.0009	2.9260 ± 0.0007	7.540 ± 0.005
14	300	33.1 ± 0.4	3.8970 ± 0.0014	2.9108 ± 0.0011	7.423 ± 0.008
15	300	36.17 ± 0.12	3.8853 ± 0.0004	2.8904 ± 0.0003	7.268 ± 0.002
16	300	36.47 ± 0.37	3.8842 ± 0.0011	2.8913 ± 0.0008	7.275 ± 0.006
17	300	39.93 ± 0.45	3.8717 ± 0.0016	2.8849 ± 0.0012	7.227 ± 0.009
18	300	42.76 ± 0.35	3.8619 ± 0.0022	2.8544 ± 0.0016	7.000 ± 0.012
19	300	42.79 ± 0.05	3.8618 ± 0.0002	2.8649 ± 0.0001	7.077 ± 0.001
20	300	43.04 ± 0.05	3.8609 ± 0.0002	2.8499 ± 0.0001	6.967 ± 0.001
21	300	60.52 ± 0.4	3.8075 ± 0.0010	2.7790 ± 0.0007	6.460 ± 0.005
22	348	37.53 ± 0.50	3.8813 ± 0.0018	2.8898 ± 0.0013	7.26 ± 0.01
23	352	7.74 ± 0.15	4.0249 ± 0.0010	3.2139 ± 0.0008	9.992 ± 0.007
24	356	7.77 ± 0.15	4.0249 ± 0.0010	3.2139 ± 0.0008	9.992 ± 0.007
25	397	44.74 ± 0.60	3.8569 ± 0.0030	2.8522 ± 0.0022	6.9841 ± 0.016
26	398	46.45 ± 0.40	3.8513 ± 0.0012	2.8388 ± 0.0009	6.886 ± 0.006
27	400	7.43 ± 0.15	4.0291 ± 0.0010	3.2234 ± 0.0008	10.082 ± 0.008
28	411	64.70 ± 0.80	3.7976 ± 0.0022	2.7570 ± 0.0016	6.308 ± 0.011
29	413	65.26 ± 0.90	3.7899 ± 0.0030	2.7530 ± 0.0022	6.280 ± 0.015
30	450	7.20 ± 0.12	4.0328 ± 0.0008	3.2362 ± 0.0006	10.202 ± 0.006
31	496	40.94 ± 0.33	3.8718 ± 0.0022	2.8723 ± 0.0016	7.133 ± 0.012
32	496	32.26 ± 0.05	3.9047 ± 0.0002	2.9302 ± 0.0002	7.573 ± 0.012
33	500	42.69 ± 0.22	3.8657 ± 0.0009	2.8650 ± 0.0007	7.078 ± 0.005
34	501	7.61 ± 0.44	4.0324 ± 0.0030	3.2323 ± 0.0024	10.165 ± 0.023
35	501	45.48 ± 0.62	3.8562 ± 0.0020	2.8500 ± 0.0015	6.968 ± 0.011
36	502	64.27 ± 0.90	3.7999 ± 0.0024	2.7573 ± 0.0017	6.310 ± 0.012
37	549	34.76 ± 0.06	3.8960 ± 0.0002	2.9135 ± 0.0002	7.444 ± 0.001
38	550	40.77 ± 0.22	3.8735 ± 0.0007	2.8765 ± 0.0005	7.164 ± 0.004
39	550	41.27 ± 0.25	3.8717 ± 0.0030	2.8739 ± 0.0022	7.144 ± 0.011
40	551	7.91 ± 0.02	4.0326 ± 0.0001	3.2376 ± 0.0001	10.215 ± 0.001
41	552	62.63 ± 0.55	3.8050 ± 0.0015	2.7647 ± 0.0011	6.361 ± 0.008
42	600	7.19 ± 0.26	4.040 ± 0.0020	No Ice	No Ice
43	600	32.25 ± 0.19	3.9172 ± 0.0008	2.9356 ± 0.0006	7.615 ± 0.005
44	600	40.08 ± 0.42	3.8769 ± 0.0016	2.8818 ± 0.0012	7.204 ± 0.009
45	600	40.25 ± 0.30	3.8763 ± 0.0029	2.8823 ± 0.0022	7.208 ± 0.016
46	600	41.03 ± 0.10	3.8735 ± 0.0006	2.8745 ± 0.0004	7.149 ± 0.003
47	601	58.67 ± 0.56	3.8168 ± 0.0016	2.7849 ± 0.0012	6.502 ± 0.008
48	602	34.97 ± 0.90	3.8963 ± 0.0035	2.9156 ± 0.0026	7.460 ± 0.020
49	650	29.60 ± 0.35	3.9195 ± 0.0015	2.9609 ± 0.0011	7.814 ± 0.009
50	650	37.57 ± 0.32	3.8873 ± 0.0012	2.9015 ± 0.0009	7.352 ± 0.007
51	650	53.63 ± 0.90	3.8325 ± 0.0022	2.8089 ± 0.0016	6.671 ± 0.011
52	651	28.85 ± 0.65	3.9228 ± 0.0024	2.9666 ± 0.0018	7.859 ± 0.014
53	651	39.59 ± 0.29	3.8803 ± 0.0011	2.8858 ± 0.0008	7.234 ± 0.006
54	652	54.36 ± 0.17	3.8303 ± 0.0005	2.8061 ± 0.0004	6.651 ± 0.003
55	700	37.67 ± 0.18	3.8880 ± 0.0007	2.9014 ± 0.0005	7.352 ± 0.004
56	700	39.1 ± 0.4	3.7999 ± 0.0024	2.8935 ± 0.0018	7.292 ± 0.014
57	700	48.52 ± 0.23	3.8496 ± 0.0006	2.8380 ± 0.0005	6.881 ± 0.003
58	701	26.78 ± 0.32	3.9334 ± 0.0008	2.9918 ± 0.0006	8.061 ± 0.005
59	701	39.15 ± 0.32	3.8824 ± 0.0004	2.8953 ± 0.0003	7.306 ± 0.002
60	750	36.64 ± 0.43	3.8993 ± 0.0017	2.9160 ± 0.0013	7.464 ± 0.010
61	750	36.89 ± 0.54	3.8993 ± 0.0017	2.9114 ± 0.0013	7.428 ± 0.010
62	750	44.68 ± 0.40	3.8634 ± 0.0010	2.8663 ± 0.0008	7.088 ± 0.006
63	751	25.12 ± 0.33	3.9425 ± 0.0015	3.0095 ± 0.0011	8.205 ± 0.009
64	783	23.37 ± 0.31	3.9519 ± 0.0015	No Ice	No Ice
65	791	21.86 ± 0.39	3.9598 ± 0.0021	No Ice	No Ice
66	798	36.53 ± 0.03	3.8943 ± 0.0009	2.9204 ± 0.0007	7.497 ± 0.005
67	803	44.46 ± 0.60	3.7999 ± 0.0024	2.8685 ± 0.0018	7.104 ± 0.013
68	810	36.27 ± 0.40	3.8957 ± 0.0030	2.9208 ± 0.0022	7.500 ± 0.017
69	852	42.59 ± 0.30	3.8993 ± 0.0017	2.8872 ± 0.0013	7.245 ± 0.009
70	860	32.02 ± 0.33	3.9143 ± 0.0014	No Ice	No Ice
71	902	36.59 ± 0.10	3.8965 ± 0.0004	No Ice	No Ice

[a] Temperature is in Kelvin and was determined by placing a thermocouple between the diamond and rhenium gasket. Pressure is presented in GPa and was ascertained from the measured lattice parameter for gold. The lattice parameter for gold is presented as the mean value of the {111}, {200} and {220} diffraction lines whereas the uncertainty is the 2σ standard deviation from the mean. The uncertainties listed for pressure and the volumetric data of Ice VII were determined by propagation of the uncertainty in the gold lattice parameter.

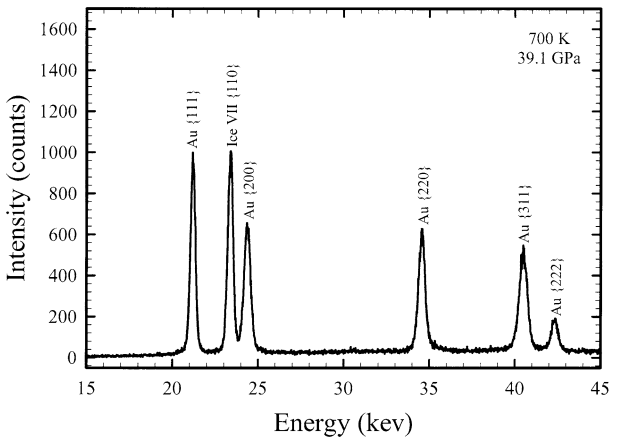

Fig. 3. This figure is from experiment 56 and is an energy dispersive X-ray diffraction pattern of Ice VII and gold at elevated temperature (700 K) and elevated pressure (39.1 ± 0.4 GPa). The data were collected as a function of energy (keV) at a $2\theta = 15°$. Ice VII and gold diffraction lines are labeled accordingly. The disappearance of the Ice VII diffraction lines, most notably that of {110}, were used to indicate melting in the H_2O phase system.

$$P(\text{GPa}) = 3/2K_{T0}\left[(V_0/V)^{7/3} - (V_0/V)^{5/3}\right] \times \left[1 - 3/4(4 - K'_{T0})((V_0/V)^{2/3} - 1)\right] \quad (2)$$

where K_{T0}, K'_{T0} and V_0 are the isothermal bulk modulus, its pressure derivative and the volume at zero pressure, respectively. V_0 was constrained by the compression data alone because Ice VII is a high-pressure nonquenchable phase. The data presented here extend over a compression range, defined as ($V_0 - V/V_0$), of 0.18 to 0.48. The fit of data using the third-order Birch-Murnaghan equation of state was conducted using two methodologies, the first was to allow all variables (K_{T0}, K'_{T0} and V_0) to be independent, and the second was to set the zero-pressure volume to a constant and to solve for K_{T0} and K'_{T0}. Solving simultaneously for all three variables produced $V_0 = 12.4 \pm 0.1$ cm^3/mol, $K_{T0} = 21.1 \pm 1.3$ GPa, and $K'_{T0} = 4.4 \pm 0.1$. Overall, the result are in good agreement with the studies of Wolanin et al. (1997), Fei et al. (1993), Hemley et al. (1987) and Munro et al. (1982) whereas the volumes measured by Liu (1982) are systematically depressed over the entire pressure range. The values of V_0, K_{T0} and K'_{T0} used in this study will be those obtained by solving simultaneously since they best represent the data and the uncertainty associated with data.

3.2. X-ray Diffraction Data of Ice VII at Elevated Pressures and Temperatures

X-ray diffraction data for Ice VII and gold were collected at 50 degree intervals during heating so that the thermal expansion data could be analyzed in light of the effects of pressure and temperature. A typical diffraction pattern observed is illustrated in Figure 3. The thermal expansion was found to be significant at pressure below ~15 GPa, but decreased drastically at higher pressures. Typically, the thermal expansion of any mineral at ambient pressure, $\alpha_0(T)$, can be obtained simply through heating and can be expressed as a linear function of temperature through the following relation:

$$\alpha_0(T) = a_0 + a_1 T, \quad (3)$$

where a_0 and a_1 are empirical coefficients. However, since Ice VII is a nonquenchable phase we were forced to constrain our high pressure data using the volume coefficient of thermal expansion, $\alpha(P,T)$, defined as:

$$\alpha(P,T) = \alpha_0(T)\left(1 + \frac{K'_{T0}}{K_{T0}}P\right)^{-\eta} \quad (4)$$

where η is an adjustable value obtained from the effect of pressure on the volume of Ice VII at high temperatures. We fit the molar volume data at elevated pressure and temperature, $V(P,T)$, using a PVT equation of state of the form:

$$V(P,T) = V(P,300\text{ K})\exp\left[\int_{300K}^{T} \alpha(P,T)dT\right] \quad (5)$$

where $V(P,300\text{ K})$ is the molar volume at a given pressure and 300 K and was calculated using Eqn. 2. Solving Eqns. 3-5, we obtained $a_0 = -4.2 \times 10^{-4}$, $a_1 = 1.56 \times 10^{-6}$ and $\eta = 1.1$. $V(P,T)$ is best related to $V(P,300\text{ K})$ graphically by plotting the difference between the molar volume at elevated pressure and temperature from that at temperature and ambient pressure, $V(P,T) - V(P,300\text{ K})$, as a function of pressure and temperature. Figure 4 illustrates the experimental data are well reproduced using Eqns. 3-5.

3.3. Determination of the Ice VII Melting Curve

The diffraction lines and molar volume of Ice VII were monitored as a function of pressure and temperature up to the

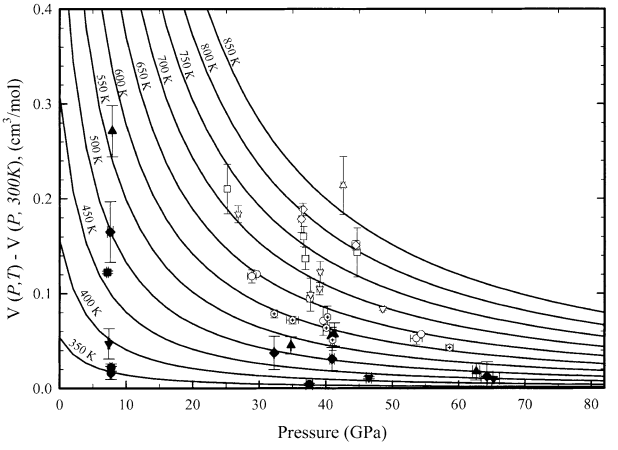

Fig. 4. The molar volume of Ice VII was determined as a function of pressure along any given isotherm to establish their interdependence. High-temperature volume data are presented in 50 degree increments relative to the volume at 300 K for clarity. The lines are isotherms calculated using the procedure outlined in Eqns. 3-5. The filled circles, inverted triangles, squares, diamonds and triangles represent data points at 350, 400, 450, 500 and 550 K, respectively. The open hexagons (filled with a black cross), circles, inverted triangles, squares, diamonds and triangles are data points at 600, 650, 700, 750, 800 and 850 K, respectively.

Table 2. Compilation of the data used to determine the melting curve of Ice VII.[a]

Experiment	Ice VII present	Temperature (K)	Pressure (GPa)	Midpoint temperature (K)	Midpoint pressure (GPa)
40	Y	551	7.91 ± 0.02		
Midpoint				576 ± 24	7.55 ± 0.36
42	N	600	7.19 ± 0.26		
63	Y	751	25.12 ± 0.33		
Midpoint				767 ± 16	24.25 ± 0.88
64	N	783	23.37 ± 0.31		
68	Y	810	36.27 ± 0.40		
Midpoint				835 ± 25	34.1 ± 2.1
70	N	860	32.02 ± 0.33		
69	Y	852	42.59 ± 0.30		
Midpoint				877 ± 25	39.6 ± 3.0
71	N	902	36.59 ± 0.10		
Midpoint				850 ± 52	36.56 ± 0.03
66	Y	798	36.53 ± 0.03		

[a] Y and N denote whether the diffraction pattern of Ice VII was observed (Y) or not observed (N). The midpoint data was determined by taking the mean of the temperature and pressure data of concurrent points in pressure-temperature space. The uncertainty for pressure and temperature of the data points are discussed in the text whereas the uncertainty of the calculated midpoint values are taken as the half-widths between data points.

melting temperature at any given pressure. The methodology employed in this study was to use the disappearance of the diffraction pattern of Ice VII to monitor the melting of Ice VII in the system. The melting curve of Ice VII was monitored predominately by using the disappearance of the 110 peak as evidence of the minimum melting temperature. The melting curve for Ice VII was defined in this study by the midpoint between Ice VII present and absent points in pressure-temperature space (Table 2). The possibility of recrystallization of Ice VII and the disappearance of the 110 line, giving a false melting result, was examined by continuing to increase the sample temperature (to check for the reappearance of the 110 line), and by reversals about the melting curve. Reversals were conducted by monitoring the 110 line during heating, until disappearance, and then cooling the sample in 50 degree increments until the line reappeared. The resulting temperatures associated with the reversals were found to be broadly consistent with those of the melting curve. The melting curve for Ice VII can be well represented in pressure-temperature space by the following Simon equation:

$$\frac{(P - 2.17)}{0.764} = \left(\frac{T}{355}\right)^{4.32} - 1 \quad (6)$$

where P is pressure (GPa) and T is temperature (K). Figure 5 illustrates the melting curve extrapolated up to 70 GPa. The melting curve of Ice VII was found to be broadly consistent with the data of Fei et al. (1993), Mishima and Endo (1978), and Pistorius et al. (1963) with predicted melting temperatures differing by less than 25 K at any given pressure (Fig. 6).

The melting curve of Ice VII was combined with the volumetric data to calculate the molar density (ρ) of Ice VII along the melting curve. The following equation represents the best-fit relationship to the data:

$$\rho(\text{mol/cm}^3) = 0.0805 + 0.0229*(1 - \exp^{(-0.0743*P)}) + 0.1573*(1 - \exp^{(-0.0061*P)}) \quad (7)$$

where ρ is in mol/cm^3, P is pressure (GPa) and exp represents the exponential function. There is excellent agreement between the calculated molar density and the value determined for Ice VII near the melting curve.

4. DISCUSSION

4.1. Ice VII *PVT* Properties

The properties of Ice VII at 300 K has been studied in great detail with nice agreement between most of the studies. These studies have ranged from compression studies using synchrotron X-ray sources to in situ Brillouin spectroscopy on individual crystals. Shimizu et al. (1996) attempted to use Brillouin spectroscopy on a single crystal of Ice VII to determine the acoustic, adiabatic elastic constants and adiabatic bulk modulus. However, it must be noted that Ice VII in a diamond anvil

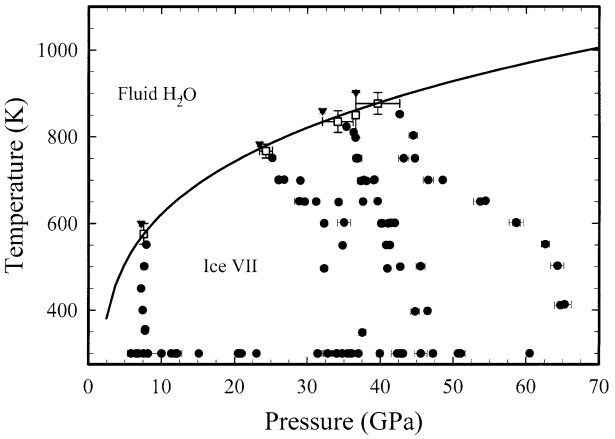

Fig. 5. The melting curve of Ice VII is presented as a function of pressure and temperature. The circles and inverted triangles represent points in pressure-temperature space where X-ray peaks characteristic of Ice VII were present or absent, respectively. The open squares represent the midpoints between concurrent Ice VII-preset and absent positions and were used to define the melting curve (solid line). The solid line is the melting curve of Ice VII is related by a Simon equation.

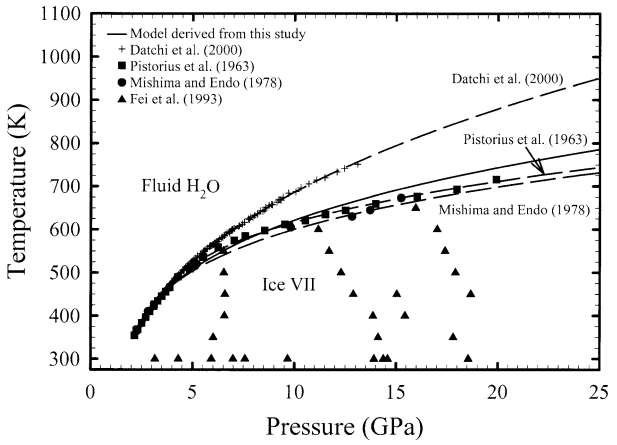

Fig. 6. Comparison of the results from previous studies to the one presented here, signified by the solid line, up to 25 GPa. The data indicate that all studies agree up to approximately 600 K and 7 GPa. The dashed lines are the Ice VII melting curve models of Datchi et al. (2000), Mishima and Endo (1978), and Pistorius et al. (1963) and are labeled accordingly. The divergence seen in the data of Datchi et al. (2000) to higher temperatures for any given pressure results in an overestimation of the melting temperature relative to this study; however, it must be noted that they only have data to 13 GPa so our main contention is with the model they proposed to fit their data. A similar situation exists for the studies of Fei et al. (1993), Mishima and Endo (1978), and Pistorius et al. (1963), the melting curve data they present range to approximately 16, 17 and 20 GPa, respectively, and are broadly consistent with the model presented here, but their extrapolations to higher pressures suggest that those studies underestimate the melting temperature above 20 GPa.

cell is usually polycrystalline and growing a single crystal is difficult. Shimizu et al. (1996) used a pressure-temperature path that crossed into the Ice VII stability region at a point above the fluid H_2O-Ice VI-Ice VII triple point to obtain a singe crystal. Their data are based on a single crystal where no crystal facets were observed. They report a bulk modulus for Ice VII that is in good agreement with a previous X-ray study (Munro et al., 1982).

X-ray diffraction data have provided the bulk of data on Ice VII with Loubeyre et al. (1999) presenting data over the largest compression range. They monitored the H_2O system up to 170 GPa and fit a Vinet form equation to their data. A zero-pressure volume, bulk modulus and its pressure derivative were calculated as 14.52 (cm^3/mol), 4.26 GPa, and 7.75. Their results were based on X-ray diffraction obtained from a single crystal.

Wolanin et al. (1997) studied polycrystalline Ice VII in a diamond anvil cell up to 106 GPa using angle dispersive X-ray diffraction. They fit the compression data using both Birch-Murnaghan and Vinet equations of state and constraining the bulk modulus to 14.9 ± 0.8 GPa, following the work of Shimizu et al. (1996). Wolanin et al. (1997) used their data and the bulk modulus taken from Shimizu et al. (1996) to calculate the zero pressure volume and the pressure derivative of the bulk modulus. Values for the zero pressure volume and bulk modulus pressure derivative were reported as 12.37 ± 0.09 and 5.4 ± 0.1 for the Birch-Murnaghan solution and 12.11 ± 0.09 and 6.2 ± 0.1, respectively, for the Vinet solution.

Hemley et al. (1987) studied Ice VII up to 128 GPa which corresponded to a compression ratio of 0.13 (4.3 GPa) to 0.58. They suggest that the zero-pressure volume, bulk modulus and its pressure derivative were 12.3 ± 0.3 (cm^3/mol), 23.7 ± 0.9 GPa, and 4.15 ± 0.07, respectively. Whereas the study of Hemley et al. (1987) collected compression data over and a much larger range of pressure, the slight change in the structure of Ice VII to the proposed Ice X structure at approximately 70 GPa may require the higher pressure data be excluded (Pruzan et al., 1997; Goncharov et al., 1999). Recalculating K_{T0}, K'_{T0} and V_0 for their data below 70 GPa gives values of 24.8 ± 1.2 GPa, 4.14 ± 0.12 and 12.2 ± 0.1 (cm^3/mol), respectively. Munro et al. (1982) studied the compression up to 36 GPa and used a linear ruby pressure scale to estimate pressure. Hemley et al. (1987) corrected their results to the improved nonlinear ruby scale and found excellent agreement with only a small discrepancy at low pressures. Fei et al. (1993) presented Ice VII compression data ranging from 3.16 to 18.55 GPa, and, although the compression range was not as large as that of Hemley et al. (1987) or other studies, the zero-pressure volume, bulk modulus and its pressure derivative were all within the experimental uncertainty quoted by Hemley et al. (1987). The volumetric results of Liu (1982) are systematically shifted to lower volumes for any given pressure relative to the studies previously discussed. Although he presented a bulk modulus of 24.6 ± 0.9 GPa, broadly consistent with the previous studies, the zero-pressure volume and the bulk modulus pressure derivative were 12.7 (cm^3/mol) and 4.4, respectively. Hemley et al. (1987) suggested the difference may be attributed to the large pressure gradient present between the sample and the ruby grain used to estimate pressure. However, it must be noted that Liu (1982) chose the first datum point at 2.15 GPa as his standard state which may have also systematically shifted his best fit line to lower pressures for any given pressure.

Our data closely match and are considered consistent with those of the previous studies. The zero pressure volume of Ice VII that we propose here is broadly consistent with the values reported by Hemley et al. (1987) and Fei et al. (1993). The Birch-Murnaghan treatment presented by Wolanin et al. (1997) closely reproduces our zero pressure volume but does not match our calculated bulk modulus and its pressure derivative. By setting the bulk modulus to a value derived from Shimizu et al. (1996), their pressure derivative of the bulk modulus is increased so as to fit the data. Thus, if their chosen bulk modulus is incorrect, their pressure derivative would be as well.

Previous work on the volumetric properties of Ice VII at elevated temperatures and pressures is limited to Fei et al. (1993). They collected data on Ice VII up to 650 K and 18.55 GPa and our results extend this range to 902 K and 65.26 GPa. Generally, our results are consistent with those of Fei et al. (1993) with the empirical coefficients a_0 and a_1 varying by less than 7 and 4%, respectively. Whereas our values can adequately model both data set over the entire range of pressure-temperature conditions the values presented in Fei et al. (1993) overestimated slightly the volume of Ice VII at pressure >40 GPa. This slight variation may be attributed to the large variation in the compression range of the two studies with this study, having data over a much larger pressure-temperature region, providing more tightly constrained coefficients.

4.2. Melting Curve of Ice VII

The melting curve of Ice VII has been studied by using a variety of experimental methods. Pistorius et al. (1963) carried out experiments in a high-temperature high-pressure device up to 20 GPa. They were able to determine melting by measuring the change in electrical resistance of the sample during melting. The sample, in this case, was a paste composed of calcined ferric oxide and a dilute solution of cupric sulfate. Pistorius et al. (1963) reports that temperature measurements of the melting curve can be considered accurate to ± 8 K.

Mishima and Endo (1978) utilized a multianvil apparatus and a strain-sensitive manganin wire to measure to volume change associated with melting in the Ice VII-fluid H_2O phase system. A notable increase in the resistance of the wire was considered reflective of a change in volume in the H_2O phase system and noted as melting of Ice VII. Their study extended from 3 to 15 GPa and was largely consistent with the earlier study of Pistorius et al. (1963) with only a slight discrepancy at intermediate pressures.

Recently, studies in diamond anvil assemblies have allowed for more innovative methods of detecting melting in the H_2O phase system. Fei et al. (1993) used an externally heated diamond anvil assembly and synchrotron radiation to monitor the disappearance of the diffraction lines as an indication of melting. They measured temperature by placing a thermocouple directly against the interface of the diamond and gasket. The high thermal conductivity of diamond is thought to allow a direct measurement sample temperature using an external thermocouple. The melting curve was crossed at approximately 7, 9 and 15 GPa and the results compared to those of Pistorius et al. (1963) and Mishima and Endo (1978). Generally, the models derived from data presented in the three studies compare favorably, with a variation of 12 and 17 K at 10 and 20 GPa, respectively. The general agreement of the three studies is remarkable when the large variations in the methods employed are noted.

A novel approach was undertaken by Datchi et al. (2000) when they employed in-situ techniques to measure temperature and pressure in a diamond anvil cell assembly (Datchi et al., 1997) to study the Ice VII-fluid H_2O transition. They used the shift in the $^7D_0$-$^5F_0$ fluorescence lines of SrB_4O_7:Sm^{2+} to monitor pressure and coupled this value to the shift of the R_1 ruby line to determine temperature. The R_1 shift has been know to be influenced by increases in temperature and pressure, therefore, thought to be most useful for determining pressure at 300 K. To demonstrate the reliability of the proposed method, Datchi et al. (1997) measured the argon isochore at melting up to approximately 420 K and 2.4 GPa, their results were in excellent agreement with a Simon-Glatzel based extrapolation using low pressure data. Their data for the Ice VII melting curve begins to significantly deviate at approximately 6 GPa and 550 K from the melting curve determined by the previous workers and indicates a melting temperature >100 K higher at 13 GPa (their highest pressure). The applicability of the methods developed by Datchi et al. (1997) to temperatures greater than 550 K has not been demonstrated adequately to date. A slight shift that was unaccounted for or broadening of either the ruby or SrB_4O_7:Sm^{2+} lines would cause greater uncertainty and could result in a systematic error.

The previous studies addressed the melting curve of Ice VII at pressures less than 20 GPa and are largely equivalent. Our low-pressure data, crossing the melting curve at approximately 7 GPa, is consistent with all of the previous studies. However, the models derived from the low-pressure studies and extrapolated using Simon equations to pressures greater than 20 GPa do not agree with our high-pressure data. The data indicate the transition of Ice VII to fluid H_2O occurs at greater temperatures for pressures less than 20 GPa than the models of Pistorius et al. (1963), Mishima and Endo (1978) and Fei et al. (1993) predict. The difference in the onset of melting found in this study increased from approximately 50 K at 30 GPa to approximately 75 K at 50 GPa. Extending the melting curve to 80 GPa using Equation 6 and comparing these results to the models put forth by Mishima and Endo (1978) and Pistorius et al. (1963) suggests that Ice VII will melt at 115 and 90 K higher, respectively. Comparison of our study to that of Datchi et al. (2000) indicate their model overestimates the melting temperature by approximately 275 and 375 K at 50 and 80 GPa, respectively.

Datchi et al. (2000) argued that the study of Fei et al. (1993), which employed the same methods described in this study, only provided lower limits on the melting temperature. They suggest that relying solely on the disappearance of the {110} peak could provide false melting temperatures because of recrystallization of Ice VII. We tested their hypothesis by implementing reversals about the melting curve and performing exploratory experiments in the MgO-H_2O system.

Reversal experiments were performed about the Ice VII melting curve by heating the sample until the disappearance of Ice VII diffraction lines was observed and then cooling the sample until the Ice VII diffraction lines reappeared. Table 3 lists one such set of reversals as experiment 69-71-66. These three experiments were all collected along one continuos pressure-temperature path. Experiment 69 had observable Ice VII diffraction lines at 852 K and 42.6 GPa, but these same diffraction lines were not observed in experiment 71 when the cell was heated to 902 K (there was also a substantial drop in pressure to 36.6 GPa). Cooling the experiment from 902 K to 798 K (36.5 GPa) resulted in a the reappearance of the Ice VII diffraction lines, as noted in experiment 66. It is possible that Ice VII could recrystallized at high-temperature, near the melting curve, and effectively result in an underestimation of the melting curve, however, the reappearance of the diffraction line with subsequent cooling suggests that melting was much more likely the cause of the diffraction line disappearance than recrystallization.

Exploratory experiments in the MgO-H_2O system were conducted to further test the Datchi et al. (2000) hypothesis. Small grains of MgO were placed in the sample chamber with gold and a relatively large volume of H_2O. The methodology was to monitor the disappearance of the diffraction pattern of Ice VII and the appearance of brucite, $Mg(OH)_2$, peaks following the reaction of fluid H_2O with MgO. The use of the energy dispersive technique allowed us to monitor the reaction progress. Generally, as temperature was increased, an experiment was observed to exhibit: 1) slight drop in pressure, 2) sharpening of the Ice VII diffraction lines suggesting the onset of melting, 3) the appearance of diffraction lines indicative of brucite as the relative intensities of MgO diffraction lines decreased, and 4) total disappearance of Ice VII and MgO diffraction lines and

Table 3. Comparison from select studies of the zero-pressure volume (V_0), bulk modulus (K_{T0}) and its pressure derivative (K'_{T0}) for Ice VII calculated from isothermal compression curves at 300 K[a].

Reference	Pressure range (GPa)	V_0 (cm^3/mol)	K_{T0} (GPa)	K'_{T0}
This study	6.82–60.52	12.4 ± 0.1	21.1 ± 1.3	4.4 ± 0.1
Loubeyre et al. (1999)	2.2–170	14.52	4.26	7.75
Wolanin et al. (1997*a*)	2.1–106	12.37 ± 0.09	14.9 ± 0.1[b]	5.4 ± 0.1
Wolanin et al. (1997*b*)	2.1–106	12.11 ± 0.09	14.9 ± 0.1[b]	6.2 ± 0.1
Hemley et al. (1987)	4.3–128.0	12.3 ± 0.3	23.7 ± 0.9	4.15 ± 0.07
Liu (1982)	2.15–50.4	12.7 ± 0.1	24.6 ± 0.9	4.4
Fei et al. (1993)	3.16–18.55	12.3 ± 0.2	23.9 ± 0.7	4.2 ± 0.5

[a] Wolanin et al. (1997*a*) and Wolanin et al. (1997*b*) correspond to the Birch-Murnaghan and Vinet fits, respectively, presented in that study.
[b] The bulk modulus used in the Wolanin et al. (1997) study was derived from the elastic coefficients of Shimizu et al. (1996). Wolanin et al. (1997) used their data and the bulk modulus taken from Shimizu et al. (1996) to calculate the zero pressure volume and the pressure derivative of the bulk modulus.

noticeable drop in pressure (up to approximately 2 GPa at the highest pressures). It was noted that the appearance of brucite always preceded the disappearance of the Ice VII diffraction lines. The sequence described here occurred in less than 5 min and over a temperature interval that was always less than 25 K. Our interpretation is that the formation of brucite from MgO occurred immediately as fluid H_2O became available and before all of the Ice VII had melted. The Ice VII melting curve determinations performed using this method were within the uncertainty of those which relied exclusively on the disappearance of Ice VII diffraction lines. These exploratory experiments were only conducted from starting materials of MgO and H_2O and no samples were heated multiple times. Our results do not support the hypothesis of Datchi et al. (2000), and we concluded that the disappearance of the Ice VII diffraction lines, along with select reversal experiments, are satisfactory in monitoring melting in the Ice VII-fluid H_2O phase system.

We do not find significant differences between our low-pressure data and those of previous studies. However, the predicted melting curves of Ice VII of earlier studies are not consistent with the high-pressure data presented in this study. While there is general agreement between the low-pressure data from our study and the data of others, the extrapolation they employed to high-pressures does not represent accurately the Ice VII melting curve. Therefore, since this study is the first to present data for the Ice VII–fluid H_2O phase system at pressures above 20 GPa, it should be considered the first choice for modeling the H_2O phase system at high pressures.

5. IMPLICATIONS

5.1. Ice VII in Planetary Physics

Our results can be used to place constraints on the density of both Ice VII and fluid H_2O under conditions that may exist in the interiors of icy satellites such as Ganymede and Callisto. Eqn. 7 illustrates the molar density of Ice VII along the melting curve, and combined with the *EOS* for Ice VII presented in this study, can be used to help determine the density of Ice VII and fluid H_2O as a function of pressure and temperature. These model values can be applied to icy satellites, such as Ganymede and Callisto, by using the data collected by the Galileo probe. According to Scott et al. (2002), the pressure-temperature relations that most likely exist at depth in Ganymede would not fall within the Ice VII stability field as outlined in this study. Callisto, on the other hand, due to its inferred low-level of differentiation could have Ice VII at depth within the satellite (Anderson et al., 1998).

The possible presence of Ice VII in subducting slabs has been recently hypothesized by Bina and Navrotsky (2000). They calculated thermal models of subduction zones and considered four classes of subducting slabs ranging from the young, slow, and shallow dipping extreme (age is 12×10^6 years, rate is 6 cm/yr, and dip is 30°, e.g., Cascadia) to old, fast and steep dipping slabs (age is 140×10^6 years, rate is 14 cm/yr, and dip is 60°, e.g., Tonga). They compared their thermal models to the melting curve of Ice VII determined by Datchi et al. (2000) and concluded that Ice VII was possible in two of the four classes of slabs considered. In general, old, steep and fast subducting slabs are most likely to contain H_2O as Ice VII. As has been presented in this study, the melting curve of Datchi et al. (2000) is not consistent with the data of other studies and, as a result, is a questionable choice for this type of modeling. Recalculating the work of Bina and Navrotsky (2000) using the melting curve for Ice VII presented here reduces the potential presence of Ice VII to only the coldest, steepest, and fastest slab model. Our results can not disprove the hypothesis proposed for Ice VII in subducting slabs, but the results greatly limit the environments in which Ice VII could form.

5.2. Constraining the *EOS* of Fluid H_2O

Equations of state for fluid H_2O at high-pressures (e.g., Rice and Walsh, 1957; Halbach and Chatterjee, 1982; Belonoshko and Saxena, 1991; Pitzer and Sterner, 1994; Sakane et al., 2001) have been derived mainly from shock wave experiments and theoretical models. Very few static compression studies have been conducted on fluid H_2O. A simple method for examining the pressure-volume-temperature properties of fluid H_2O at elevated pressures and temperatures is to verify the melting line of an H_2O ice, in this case Ice VII, at high pressures and temperatures. This is possible because, along the melting curve, the Gibbs free energies of formation for fluid H_2O, $\Delta G_{\text{fluid } H_2O}(P,T)$, and Ice VII, $\Delta G_{\text{Ice VII}}(P,T)$, are equivalent and denoted here as:

$$\Delta G_{\text{Ice VII}}(P,T) = \Delta G_{\text{fluid H}_2\text{O}}(P,T)\,. \quad (8)$$

The thermodynamic relations of solid H_2O can be easily related to those of the fluid H_2O through the relation:

$$\Delta G_{\text{Ice VII}}(P,T) = \Delta G^{\text{O}}_{\text{Ice VII}}(T) + \int_{1\text{ bar}}^{P} V_{\text{Ice VII}}\, dP\,. \quad (9)$$

where $\Delta G_{\text{Ice VII}}(P,T)$ and $\Delta G_{\text{Ice VII}}(T)$ are the free energies of formation at pressure and temperature and 1 bar and temperature, respectively. $\Delta G_{\text{Ice VII}}(P,T)$ was constrained by the thermodynamic formulation presented in this study. $\Delta G_{\text{Ice VII}}(T)$ at pressures less than 5 GPa was calculated using the equation of state of Ice VII presented here along with the model from Halbach and Chatterjee (1982) following the method outlined in Fei et al., 1993; Eqn. 8). The calculated melting curve agrees well with the experimental data presented here, although, it must be noted that the absence of data in the intermediate pressure range may result in slight inconsistencies (as illustrated in Fei et al., 1993).

$\Delta G_{\text{fluid H}_2\text{O}}(P,T)$ was calculated along the melting curve where $\Delta G_{\text{fluid H}_2\text{O}}(P,T)$ is equated to $\Delta G_{\text{Ice VII}}(P,T)$. This relation holds only along the melting curve. Therefore, $\Delta G_{\text{Ice VII}}(P,T)$, as constrained by the thermodynamic formulation presented in this study, was used to proxy for $\Delta G_{\text{fluid H}_2\text{O}}(P,T)$. $\Delta G_{\text{fluid H}_2\text{O}}(T)$ was calculated using the $\Delta G_{\text{fluid H}_2\text{O}}(P,T)$ values presented in Belonoshko and Saxena (1991) and the calculated volume of fluid H_2O at a given pressure and temperature on the Ice VII melting curve. We elected to use the model of Belonoshko and Saxena (1991) rather than more recent formulations (Pitzer and Sterner, 1994; Wagner and Pruss, 2002; Sakane et al., 2001) because their study was optimized to the high pressure realm and also to maintain internal consistency with Fei et al. (1993) and Fei and Mao (1993). A *modified* volume of fluid H_2O was estimated using an equation similar to Eqn. 9 and the methods described above. Model results indicate that the molar volume of fluid H_2O is over estimated by Belonoshko and Saxena (1991) at pressures greater than approximately 20 GPa, with an overestimation of approximately 0.8 cm^3/mol (approximately 10%) at 80 GPa on the Ice VII melting curve (Fig. 7). Fei and Mao (1993) estimated that the molar density of fluid H_2O was underestimated along the Ice VII melting curve by 0.52 cm^3/mol at 80 GPa, the variation between this study and the Fei and Mao (1993) study is attributed mostly to the improved melting curve determination at higher pressures present here. For example, the Ice VII melting temperature estimated by Fei et al. (1993) was ~950 K at 80 GPa, whereas we predict ~1040 K. The volumetric and thermodynamic properties of Ice VII are much more easily measured than those of fluid H_2O under similar conditions. Therefore, we concluded that our results for the melting curve of Ice VII, extended to more than double the pressure range of any previously published study, provide the best constrained method for evaluating proposed *EOS* of fluid H_2O. Although our work alone is not enough to provide an improved *EOS* for fluid H_2O future work must take account of our data.

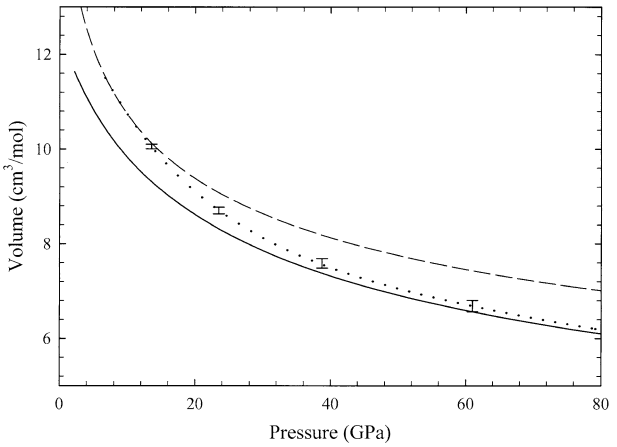

Fig. 7. Molar volume (cm^3/mol) of Ice VII, solid line, and fluid H_2O, dashed line, along the melting curve for Ice VII were calculated following the procedures outlined in the text. The solid line was calculated from the data and thermodynamic treatment presented in this study whereas the dashed line was calculated using the model of Belonoshko and Saxena (1991) combined with the thermodynamic EOS and melting curve determined in this study for Ice VII. The dotted line represents the deviation in molar volume of fluid H_2O from the Belonoshko and Saxena (1991) model from that calculated using the thermodynamic properties derived from the thermodynamic relations of Ice VII. Our results indicate that the molar volume of fluid H_2O is overestimated by the Belonoshko and Saxena (1991) model at pressures greater than approximately 20 GPa. The uncertainties in the data points were estimated assuming an uncertainty in the Ice VII melting temperature of 25 K at any given point.

6. CONCLUSIONS

Equation of state properties of Ice VII and supercritical H_2O at temperatures of 300-902 K and pressures of 6-60.5 GPa have been studied experimentally. The melting curve of Ice VII was monitored directly at a series of pressures up to 41 GPa. Our low-pressure data are consistent with the low-pressure data of others, however, our results indicate that the models extrapolated to high-pressure do not adequately represent the melting curve at pressures >20 GPa. The molar volume of Ice VII was calculated using the improved melting curve and related to the *EOS* of fluid H_2O. Our model indicates that the molar volume of fluid H_2O is overestimated in the Belonoshko and Saxena (1991) model at pressures greater than 20 GPa. These results can be used to constrain the internal order of icy satellites. Furthermore, our results limit greatly the environments in which Ice VII could form in subducting slabs.

Acknowledgments—Use of the BNL was supported by the U.S. Department of Energy, Basic Energy Sciences, Office of Science. This research is supported by the NASA grant NAG5-10537 (Y.F.) We would like to thank R. Hemley, B. Militzer, F. J. Ryerson, D. Sverjensky and an anonymous GCA reviewer for helpful comments. MRF would like to thank Henry Scott for helpful discussions regarding DAC techniques.

Associate editor: D. Sverjensky

REFERENCES

Anderson J. D., Schubert G., Jacobson R. A., Lau E. L., and Moore W. B. (1998) Distribution of rock, metals, and ices in Callisto. *Science* **280,** 1573–1576.

Anderson O. L., Isaak D. G., and Yamamoto S. (1989) Anharmonicity and the equation of state for gold. *J. Appl. Phys.* **65,** 1534–1543.

Belonoshko A. and Saxena S. K. (1991) A molecular dynamics study of the pressure-volume-temperature properties of super-critical fluids: I. H_2O. *Geochim. Cosmochim. Acta* **55,** 381–387.

Bina C. R. and Navrotsky A. (2000) Possible presence of high-pressure ice in cold subducting slabs. *Nature* **408,** 844–847.

Birch F. (1978) Finite strain isotherm and velocities for single-crystal and polycrystalline NaCl at high pressures and 300 degrees K. *J. Geophys. Res. A* **83,** 1257–1268.

Consolmagno G. J. and Lewis J. S. (1976) The evolution of icy satellite interiors and surfaces. *Icarus* **34,** 280–293.

Datchi F., LeToullec R., and Loubeyre P. (1997) Improved calibration of the SrB_4O_7: Sm^{2+} optical pressure gauge: Advantages at very high pressure and high temperatures. *J. Appl. Phys.* **81,** 3333–3339.

Datchi F., Loubeyre P., and LeToullec R. (2000) Extended and accurate determination of the melting curves of argon, helium, ice (H_2O), and hydrogen (H_2). *Phy. Rev. B* **61,** 6535–6546.

Fei Y. (1996) Crystal chemistry of FeO at high pressure and temperature. In *Mineral Spectroscopy: A Tribute to Roger G. Burns* (eds. M.-D. Dyar, C. McCammon, and M. W. Schaefer), pp. 243–254. Special Publication 5. Geochemical Society.

Fei Y. and Mao H. K. (1993) Static compression of $Mg(OH)_2$ to 78 GPa at high temperature and constraints on the equation of state of fluid H_2O. *J. Geophys. Res.* **98,** 11875–11884.

Fei Y., Mao H. K., and Hemley R. J. (1993) Thermal expansivity, bulk modulus, and melting curve of H_2O-Ice VII to 20 GPa. *J. Chem. Phys.* **99,** 5369–5373.

Goncharov A. F., Struzhkin V. V., Mao H., and Hemley R. J. (1999) Raman spectroscopy of dense H_2O and the transition to symmetric hydrogen bonds. *Phys. Rev. Lett.* **83,** 1998–2001.

Halbach H. and Chatterjee N. D. (1982) An empirical Redlich-Kwong-type equation of state for water to 1000 °C and 200 kbar. *Contrib. Mineral. Petrol.* **79,** 337–345.

Hemley R. J., Jephcoat A. P., Mao H. K., Zha C. S., Finger L. W., and Cox D. E. (1987) Static compression of H_2O-ice to 128 GPa (1.28 Mbar). *Nature* **330,** 737–740.

Kuskov O. L. and Kronrod V. A. (2001) Core sizes and internal structure of Earth's and Jupiter's satellites. *Icarus* **151,** 204–227.

Liu L. G. (1982) Compression of Ice VII to 500 kbar. *Earth Planet. Sci. Lett.* **61,** 359–364.

Loubeyre P., LeToullec R., Wolanin E., Hanfland M., and Häusermann D. (1999) Modulated phases and proton centering in ice observed by X-ray diffraction up to 170 GPa. *Nature* **397,** 503–506.

Mao H. K., Hemley R. J., Fei Y., Shu J. F., Chen L. C., Jephcoat A. P., Wu Y., and Bassett W. A. (1991) Effect of pressure, temperature, and composition on lattice parameters and density of (Fe,Mg)SiO3-perovskites to 30 GPa. *J. Geophys. Res. Lett.* **96,** 8069–8079.

Meng Y., Weidner D. J., and Fei Y. (1993) Deviatoric stress in a quasi-hydrostatic diamond anvil cell: Effect on the volume-based pressure calibration. *Geophys. Res. Lett* **20,** 1147–1150.

Mishima O. and Endo S. (1978) Melting curve of Ice VII. *J. Chem. Phys.* **68,** 4417–4418.

Munro R. G., Block S., Mauer F. A., and Piermarini G. (1982) Isothermal equations of state for H_2O-VII and D_2O-VII. *J. Appl. Phys.* **53,** 6174–6178.

Pistorius C. W. F. T., Pistorius M. C., Blakey J. P., and Admiraal L. J. (1963) Melting curve of Ice VII to 200 kbar. *J. Chem. Phys.* **38,** 600–602.

Pitzer K. S. and Sterner S. M. (1994) Equations of state valid continuously from zero to extreme pressures for H_2O and CO_2. *J. Chem. Phys.* **101,** 311–3116.

Pruzan P., Wolanin E., Gauthier M., Chervin J. C., and Canny B. (1997) Raman scattering and X-ray diffraction of ice in the megabar range. Occurrence of symmetric disordered solid above 62 GPa. *J. Phys. Chem.* **101,** 6230–6233.

Reynolds R. T. and Cassen P. M. (1979) On the internal structure of the major satellites of the outer planets. *Geophys. Res. Lett.* **6,** 121–124.

Rice M. H. and Walsh J. M. (1957) Equation of state of H_2O to 250 kilobars. *J. Chem. Phys.* **26,** 824–830.

Sakane S., Liu W., Doren D. J., Shock E. L., and Wood R. H. (2001) Prediction of the Gibbs energies and an improved equation of state for water at extreme conditions from ab initio energies with classical simulations. *Geochim. Cosmochim. Acta* **65,** 4067–4075.

Saxena S. K. and Fei Y. (1987) High pressure and high temperature fluid fugacities. *Geochim. Cosmochim. Acta* **51,** 783–791.

Schubert G., Stevenson D. J., and Ellsworth K. (1981) Internal structures of the Galilean satellites. *Icarus* **47 (*1*),** 46–59.

Scott H. P., Williams Q., and Ryerson F. J. (2002) Experimental constraints on the chemical evolution of large icy satellites. *Earth Planet. Sci. Lett.* **203,** 399–412.

Shimizu H., Nabetani T., Nishiba T., and Sasaki S. (1996) High-pressure elastic properties of the VI and VII phases of ice in dense H_2O and D_2O. *Phys. Rev. B* **53,** 6107–6110.

Stixrude L. and Bukowinski M. (1990) Fundamental thermodynamic relations and silicate melting with implications for the constitution of D. *J. Geophys. Res. B* **95,** 19311–19325.

Wagner W. and Pruss A. (2002) The IAPWS formulation 1995 for the thermodynamic properties of ordinary water substance for general and scientific use. *J. Phys. Chem. Ref. Data* **31,** 387–535.

Wolanin E., Pruzan Ph., Chervin J. C., Canny B., Gauthier M., Häusermann D. and Hanfland M. (1997) Equation of state of ice VII up to 106 GPa. *Phys. Rev. B* 56, 5781-5785.